

Probing Warm-Hot Intergalactic Medium Associated with the Virgo Cluster using an Oxygen Absorption Line

Ryuichi FUJIMOTO, Yoh TAKEI, Takayuki TAMURA,
Kazuhisa MITSUDA, and Noriko Y. YAMASAKI

*Institute of Space and Astronautical Science, Japan Aerospace Exploration Agency,
3-1-1 Yoshinodai, Sagamihara, Kanagawa 229-8510
fujimoto@astro.isas.jaxa.jp*

Ryo SHIBATA

*Department of Physics, Nagoya University, Furo-cho, Chikusa-ku, Nagoya 464-8602
Takaya OHASHI and Naomi OTA**

*Department of Physics, Tokyo Metropolitan University, 1-1 Minami-Osawa, Hachioji, Tokyo 192-0397
Michael D. AUDLEY*

*UK Astronomy Technology Centre, Royal Observatory, Blackford Hill, Edinburgh, EH9 3HJ, UK
and*

*Richard L. KELLEY and Caroline A. KILBOURNE
NASA Goddard Space Flight Center, Greenbelt MD 20771, USA*

(Received 2004 May 9; accepted 2004 August 10)

Abstract

To detect a warm-hot intergalactic medium associated with the large-scale structure of the universe, we observed a quasar behind the Virgo cluster with XMM-Newton. With a net exposure time of 54 ks, we marginally detected an O VIII $K\alpha$ absorption line at $650.9_{-1.9}^{+0.8}$ eV in the RGS spectra, with a statistical confidence of 96.4%. The observed line center energy is consistent with the redshift of M87, and hence the absorber is associated with the Virgo cluster. From the curve of growth, the O VIII column density was estimated to be $\gtrsim 7 \times 10^{16} \text{ cm}^{-2}$. In the EPIC spectra, excess emission was found after evaluating the hot intracluster medium in the Virgo cluster and various background components. We inspected the ROSAT All-Sky Survey map of the diffuse soft X-ray background, and confirmed that the level of the north and west regions just outside of the Virgo cluster is consistent with the background model that we used, while that of the east side is significantly higher and the enhancement is comparable with the excess emission found in the EPIC data. We consider a significant portion of the excess emission to be associated with the Virgo cluster, although a possible contribution from the North Polar Spur cannot be excluded. Using the column density and the emission measure and assuming an oxygen abundance of 0.1 and an ionization fraction of 0.4, we estimate that the mean electron density and the line-of-sight distance of the warm-hot gas are $\lesssim 6 \times 10^{-5} \text{ cm}^{-3}$ and $\gtrsim 9 \text{ Mpc}$, respectively. These numbers strongly suggest that we have detected a warm-hot intergalactic medium in a filament associated with the Virgo cluster.

Key words: cosmology: large-scale structure of universe — cosmology: observations — galaxies: clusters: individual (Virgo) — galaxies: intergalactic medium — galaxies: quasars: absorption lines.

1. Introduction

From several independent measurements — cosmic microwave background anisotropy analysis (Spergel et al. 2003), primordial deuterium-to-hydrogen ratio (Burles et al. 2001), and Ly α forest absorption at high redshift ($z \sim 3$) (Rauch et al. 1997) — the cosmic baryon density is now converging to $\Omega_b \approx 0.04 h_{70}^{-2}$, where $h_{70} = H_0/70 \text{ km s}^{-1} \text{ Mpc}^{-1}$ and H_0 is the Hubble constant. The local baryon density appears, however, to be far lower than these indications (e.g., Fukugita et al. 1998; Bristow, Phillipps 1994; Persic, Salucci 1992). Recent large-scale galaxy formation simulations predict that most

of the baryons ($\sim 50\%$) at the present time reside in a warm-hot intergalactic medium (WHIM) with temperatures of 10^5 – 10^7 K, and form filamentary structures associated with clusters and groups of galaxies (e.g., Cen, Ostriker 1999). This warm-hot gas is heated primarily by shock heating of gas accreting onto the large-scale structure (Davé et al. 2001), and its fraction is increasing with time. Therefore, detecting those warm-hot baryons is very important, not only for settling the ‘missing baryon’ problem, but also for understanding the formation of large-scale cosmological structure.

Considering the elemental abundance and the ionization fraction, O VII and O VIII absorption lines are the best tracers for probing the warm-hot gas at 10^6 – 10^7 K (Perna, Loeb 1998; Fang, Canizares 2000). In fact, these lines have been detected with grating spectrometers on-

* Present Address: Cosmic Radiation Laboratory, RIKEN, 2-1 Hirosawa, Wako, Saitama 351-0198

Table 1. Observation mode and net exposure time.

Instrument	Mode	Filter	Net exposure
RGS	Spectrum+Q	—	53.8 ks
EPIC pn	Full frame	Thin1	44.9 ks
EPIC MOS	Full frame	Medium	56.9 ks

board Chandra and XMM-Newton, toward PKS 2155–304, 3C 273, Mrk 421, and 3C 120 (Nicastro et al. 2002; Fang et al. 2002; Rasmussen et al. 2003; Fang et al. 2003; McKernan et al. 2003). In most cases, the center energy is consistent with a zero redshift, which suggests detection of the WHIM in the local group. However, if its redshift is zero, distinguishing it from the warm-hot interstellar matter in our Galaxy is not trivial (Futamato et al. 2004). On the other hand, soft X-ray emission in clusters of galaxies has been studied (e.g., Kaastra et al. 2003; Finoguenov et al. 2003). These authors claimed the detection of a warm-hot component with $kT \sim 0.2$ keV. However, since the energy band below 0.5 keV is significantly contaminated by emission from the Milky Way halo and the Local Hot Bubble, a precise determination of the quantities of the warm-hot gas is very difficult with the limited energy resolution of proportional counters and X-ray CCDs.

In searching for a breakthrough, we decided to probe the warm-hot gas *associated with nearby clusters of galaxies* through absorption lines by observing a quasar behind the Virgo cluster with the Reflection Grating Spectrometer (RGS; den Herder et al. 2001) onboard XMM-Newton (Jansen et al. 2001). In this paper, we report on our observation and results. We assume $h_{70} = 1$ throughout this paper. Errors are quoted at the 90% confidence level, unless otherwise stated.

2. Sample Selection and Observation

To find an appropriate target, we searched the ROSAT All-Sky Survey (RASS) bright source catalogue (Voges et al. 1999) and the source catalogue from pointed PSPC observations¹ for bright quasars behind the Virgo and Coma clusters. The target that we selected was LBQS 1228+1116. The location of this quasar is ($12^{\text{h}}30^{\text{m}}54^{\text{s}}.1$, $11^{\circ}00'11''$), which is $83'.3$ (or 0.45 Mpc in linear scale) south of M87 (figure 1). Because the redshift is $z = 0.237$ (Hewett et al. 1995), it is located well behind the Virgo cluster. The ROSAT PSPC count rate was 0.12–0.15 cps.

The observation was performed with XMM-Newton, from 2003 July 13 to July 14. The observation ID is 0145800101. The instrument mode, filter, and the net exposure time are summarized in table 1. Note that, although 100 ks was scheduled, the net observation time was only ~ 50 ks due to background flares.

¹ <http://www.xray.mpe.mpg.de/cgi-bin/rosat/rosat-survey/>

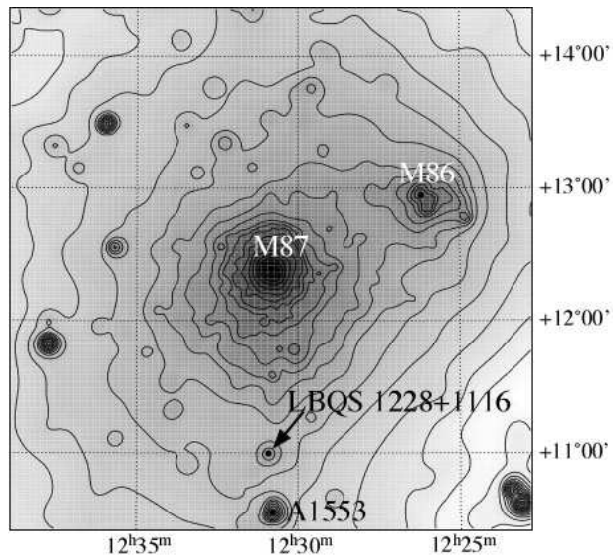


Fig. 1. ROSAT PSPC image around M87. The target, LBQS 1228+1116, is located $83.3'$ south of M87.

3. Data Analysis and Results

3.1. Absorption Line

The observation data file (ODF) was divided into two files. We performed data reduction using the XMM-Newton Science Analysis System (SAS), version 5.4.1, with standard parameters. For the RGS, we checked the data from a source-free region of CCD 9 for background flares, and accumulated the signal photons only when the count rates in this region were less than 0.15 cps for both RGS1 and 2. The net exposure time was 8.8 ks for the first file and 45.0 ks for the second. The background spectra were produced using the same data sets. All of the spectra were binned in four-channel bins (0.042 \AA), and the first and second halves were summed.

There was no sign of an O VII absorption line at around 21.6 \AA , where only the RGS1 operates. The 99.7% upper limit of the equivalent width was 2.8 eV at 21.69 \AA (571.6 eV). Therefore, we concentrated on the O VIII region. Figure 2 shows the spectra obtained with the RGS1 and 2, between 18 \AA and 20 \AA . There is an absorption-line feature at around 19.1 \AA in both RGS1 and 2. We fitted the spectra with a power law and a negative Gaussian, multiplied by the Galactic absorption ($N_{\text{H}} = 2.15 \times 10^{20} \text{ cm}^{-2}$), using XSPEC version 11.2. Since the number of photons, especially near the absorption line, is small, we used the C-statistic (maximum-likelihood) method. When this method is used, a background spectrum cannot be subtracted from the data. Therefore we estimated the background level by fitting the background spectra of RGS1 and 2 simultaneously with a constant model, and included it in the fitting model. The results are summarized in table 2; the best-fit model is shown in figure 2. The line shape was consistent with a narrow line, with a 90% upper limit on a width of $\sigma < 5.1 \text{ eV}$. Hence, the line width was fixed at 0.1 eV, which is small

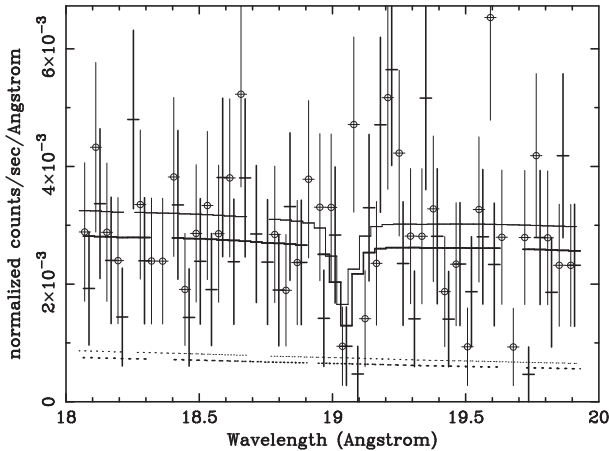


Fig. 2. Spectra around the O VIII K α line obtained with RGS1 and 2. The cross and circle symbols represent the data points of RGS1 and 2, respectively. The thick and thin solid histograms show the best-fit models for RGS1 and 2. The backgrounds were not subtracted, but were instead simultaneously fitted with a constant model. The background levels are shown with dotted curves. For illustrative purposes, channels with flickering pixels were masked.

Table 2. Best-fit parameters of the absorption line.

Absorption line	
Energy	$650.9^{+0.8}_{-1.9}$ eV
Width (σ)*	< 5.1 eV (90%)
Normalization	$(3.9^{+2.0}_{-2.8}) \times 10^{-6}$ photons $\text{cm}^{-2} \text{s}^{-1}$
Power law	
Index	3.2
Normalization †	$(3.57 \pm 0.35) \times 10^{-4}$
C-statistic	177.02
d.o.f	167

* For all fits except for the determination of the statistical error for this parameter, it was fixed at 0.1 eV.

† In units of photons $\text{keV}^{-1} \text{cm}^{-2} \text{s}^{-1}$ at 1 keV.

compared with the detector resolution ($\Delta\lambda \sim 0.06\text{--}0.07$ Å or $\Delta E \sim 2$ eV FWHM). When we calculated the errors of the absorption-line parameters, we also fixed the photon index of the power-law component. The observed line center energy and equivalent width were $650.9^{+0.8}_{-1.9}$ eV and $2.8^{+1.3}_{-2.0}$ eV, respectively. If we assume that this is an O VIII absorption line, the energy shift from the rest frame is $2.7^{+0.8}_{-1.9}$ eV, which corresponds to $cz = 1253^{+881}_{-369}$ km s^{-1} . This is consistent with that of M87 ($cz = 1307$ km s^{-1}). Note that the systematic error in the absolute energy scale of the RGS is 8 mÅ (rms) or 0.3 eV at 650 eV (den Herder et al. 2001), which is much smaller than the statistical errors.

We evaluated the statistical significance of the absorption line in the following way. The best-fit model without an absorption line gives a C-statistic of 181.76. When we include an absorption line, but fix the center and the width to the energy of the O VIII K α resonant line with $cz = 1307$ km s^{-1} and $\sigma = 0.1$ eV, respectively, we obtain

the best-fit C-statistic of 177.43. Thus, the improvement, ΔC , is 4.33. The value of ΔC approximately follows the χ^2 statistic for 1 degree of freedom if the absorption line is just a statistical fluctuation (Cash 1979). In order to evaluate the statistical confidence of the line detection, we produced 10000 simulation spectra using the continuum model shown in table 2 and the background without the absorption line. We then fitted the spectra with and without a Gaussian absorption or emission line model. We obtained $\Delta C \geq 4.33$ for 3.6% of the simulation spectra. This is consistent with the value expected from the χ^2 distribution (3.7%). We thus conclude that the chance probability for detecting such an absorption line at the very wavelength corresponding to O VIII K α at the cluster redshift is 3.6%; in other words, the statistical confidence of the absorption line is 96.4%.

The width of the wavelength range where both the RGS1 and 2 operate is ~ 15.6 Å. Because the wavelength resolution is ~ 0.06 Å, there are about 260 independent wavelength bins. The probability for detecting an emission/absorption structure of $\Delta C \geq 4.33$ at *some* wavelength is almost unity with an expected occurrence of 9.4. We searched for such structures in the observed spectra, and actually found seven such structures other than that at 19.05 Å. However, none of them can be identified with any atomic emission/absorption line with a reasonable oscillator strength at $z=0$, the cluster redshift, or the quasar redshift. Thus, these are all considered to be statistical fluctuations, and only the 19.05 Å feature can be real at a statistical confidence of 96.4%.

We then investigated the systematic errors. First, we checked the RGS spectra of bright X-ray sources in the archival data to ensure that there is no instrumental feature at that wavelength. Then, since the estimation of an absorption line could be influenced by the determination of the continuum, we examined the dependence of the equivalent width on the wavelength region used in the fits and the choice of the continuum model. For this purpose, we changed the width of the wavelength band for fits from 1.0 to 2.8 Å and added a fifth-order polynomial to the continuum. We found that, as long as the width of the fitting region is wider than 1.6 Å, the variation of the equivalent width is smaller than 0.2 eV. When the fitting region is too narrow, the continuum level is not well constrained, and is strongly coupled to the equivalent width of the line.

Assuming that the absorption line is not saturated, the equivalent width is related to the ion column density in the following way:

$$EW = \frac{\pi h e^2}{m_e c} f_{os} \frac{N_{ion}}{1+z}, \quad (1)$$

where N_{ion} is the column density of the ion and f_{os} is the oscillator strength of the transition (Sarazin 1989). We used $f_{os} = 0.70$ for the O VII resonance absorption line and $f_{os} = 0.42$ for that of O VIII (Verner et al. 1996). Then, the O VIII column density was $(6.2^{+3.3}_{-4.4}) \times 10^{16}$ cm^{-2} , while the 99.7% upper limit on the O VII column density was 3.7×10^{16} cm^{-2} .

3.2. Excess Emission

We also analyzed the EPIC data, and searched for diffuse emission. Since we are mostly interested in the low-energy band, the pn detector is suitable for our analysis. Hence, we describe the results obtained from the pn data here. We confirmed that the MOS data gave similar results, but with larger errors.

The number of events above 10 keV is regarded as a good indicator of the internal background. Thus, we discarded the data where the rate of pattern 0 events in this energy range was larger than 0.7 cps. Then, we excluded LBQS 1218+1116 and other point sources using SAS edetect_chain, and accumulated photons from the diffuse emission in the 0.3–3 keV band over the field of view. To remove any contribution from the internal background, we subtracted data taken with the filter wheel in the closed position from the spectrum. We then modeled it with four components: hot intracluster medium (ICM) of the Virgo cluster, cosmic X-ray background (CXB), Milky Way halo (MWH), and Local Hot Bubble (LHB). For the CXB, MWH, and LHB, we used parameters obtained by Lumb et al. (2002) as a template. When we fixed the temperature of the MWH (0.20 keV), the temperature of the LHB (0.07 keV), and all of the CXB parameters, the temperature of the ICM determined by the fit became $2.0^{+0.2}_{-0.1}$ keV, which is consistent with that obtained with ASCA (2.14 ± 0.12 keV, Shibata et al. 2001). The normalization of the MWH was, however, a factor of 2.3-times larger than that obtained by Lumb et al. (2002). From an analysis of eight data sets obtained with XMM-Newton, Lumb et al. (2002) indicated that the mean deviation of 0.2–1 keV flux is about 35% from field to field. Therefore, the level of the warm-hot emission around LBQS 1228+1116 is significantly higher than that of the typical Galactic background, even if we consider its fluctuation. We fixed the parameters of the MWH, LHB, and CXB to those obtained by Lumb et al. (2002), added another optically-thin thermal plasma component, and fitted the entire spectrum. Note that the normalization of the additional component (N) strongly couples with the oxygen abundance (A), and $A \times N$ is a good parameter. Here, we assumed $A = 0.1$. The results are summarized in table 3, and the best-fit models are shown in figure 3. Note that the errors given in table 3 do not contain the uncertainties of the background components. The normalization of the excess emission depends on the normalization, abundance, and temperatures of the MWH and LHB, while the temperature of the excess emission is sensitive to those of the MWH and LHB.

It is known that the Virgo cluster is located close to the North Polar Spur (Loop I) (e.g., Irwin, Sarazin 1996). To evaluate its effect, we inspected the RASS 3/4 keV map of the diffuse X-ray background (Snowden et al. 1997). The upper panel of figure 4 shows a $25^\circ \times 25^\circ$ image centered at LBQS 1228+1116. The lower panel is a projection of the $0.5^\circ \times 50^\circ$ region shown in the upper panel. The levels of the background components (MWH, LHB, CXB) estimated from the data obtained by Lumb et al. (2002) and

Table 3. Best-fit parameters of the emission spectrum*.

Intracluster medium (ICM)	
Temperature kT	$2.17^{+0.14}_{-0.16}$ keV
Normalization N^\dagger	$(3.0 \pm 0.2) \times 10^{-3}$
Abundance A	$0.22^{+0.07}_{-0.05}$
Excess emission	
Temperature kT	0.21 ± 0.01 keV
Normalization N^\dagger	$(1.5 \pm 0.2) \times 10^{-3}$
Abundance A	0.1 (fixed)
χ^2	205.36
d.o.f.	146

* The parameters of the background components were fixed at the values obtained by Lumb et al. (2002). Errors do not contain systematic errors of the background components.

\dagger In units of $10^{-14}/4\pi(D_A(1+z))^2 \int n_e^2 dV$, where D_A is the angular size distance to the source (cm) and n_e is the electron density (cm^{-3}).

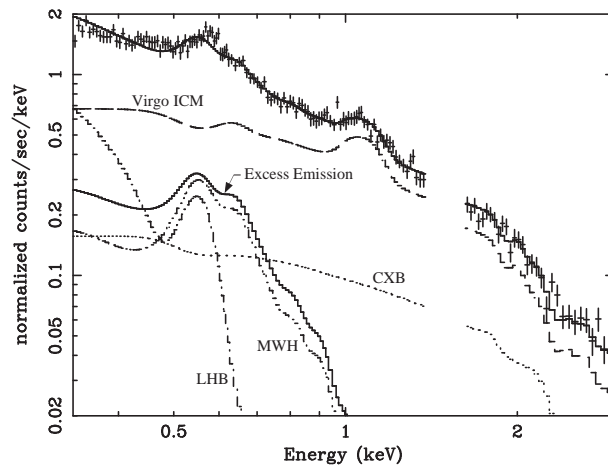


Fig. 3. Soft X-ray spectrum of the diffuse emission obtained with EPIC pn. The aluminum line region was masked. Internal background was subtracted using data taken with a filter wheel in the closed position. The parameters of the cosmic X-ray background (CXB), Milky Way halo (MWH), and Local Hot Bubble (LHB) were fixed to those obtained by Lumb et al. (2002). The data require another component that can be modeled with an optically thin thermal plasma with $kT = 0.21$ keV.

of the warm-hot emission plus LHB and CXB estimated from the present EPIC pn data are also shown in the panel with a dashed line and a solid line, respectively. The level of the west side of the Virgo cluster ($\lesssim -3^\circ$) is consistent with that of Lumb et al. (2002), while that of the east side ($\sim +4^\circ$) is significantly higher and comparable with the level of the warm-hot emission plus LHB and CXB at LBQS 1228+1116.

4. Discussion

Our results suggest the existence of a red-shifted O VIII resonance absorption line with a statistical confidence of 96.4% due to limited statistics. The velocity shift is

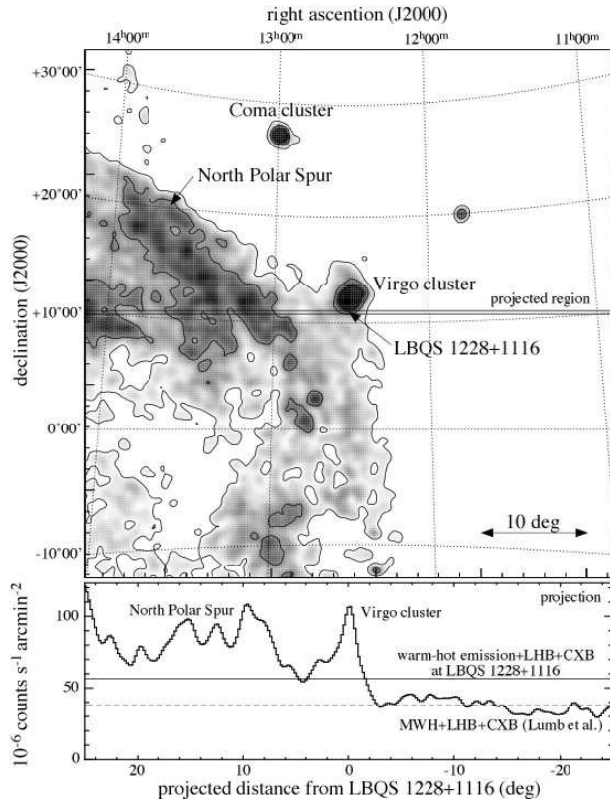


Fig. 4. (Upper panel) $25^\circ \times 25^\circ$ image centered at LBQS 1228+1116, obtained from the RASS 3/4 keV map of the diffuse X-ray background (Snowden et al. 1997). The contours represent $80, 120,$ and $180 \times 10^{-6} \text{ counts s}^{-1} \text{ arcmin}^{-2}$. (Lower panel) Projection of the $0.5^\circ \times 50^\circ$ region shown in the upper panel. The solid line represents the level of the warm-hot emission plus LHB and CXB estimated from the present EPIC data, while the dashed line represents the background level (MWH, LHB, CXB) estimated from Lumb et al. (2002).

$1253_{-369}^{+881} \text{ km s}^{-1}$, which is consistent with that of M87 ($cz = 1307 \text{ km s}^{-1}$). Thus, we claim detection of the WHIM associated with the Virgo cluster. The equivalent width of the O VIII $K\alpha$ line is $2.8_{-2.0}^{+1.3} \text{ eV}$. This is much larger than those reported for WHIM in the local group ($EW = 0.1\text{--}0.4 \text{ eV}$; e.g., Rasmussen et al. 2003; Fang et al. 2002). The intrinsic width of the line was not resolved, with an upper limit of $\sigma < 5.1 \text{ eV}$ (90%). This corresponds to a Doppler b parameter of $< 3300 \text{ km s}^{-1}$. Because the Virgo cluster is thought to be elongated along the line of sight by 12–30 Mpc (Yasuda et al. 1997), a velocity difference of 800–2100 km s^{-1} is expected due to cosmological expansion. On the other hand, a turbulent velocity of a few hundred km s^{-1} is expected for WHIM from simulations (e.g., Cen, Ostriker 1999). From the curve of growth of the O VIII $K\alpha$ absorption line (see Futamoto et al. 2004), the O VIII column density $N_{\text{O VIII}}$ is estimated to be 6.8×10^{16} , 9.6×10^{16} , and $2.4 \times 10^{17} \text{ cm}^{-2}$, respectively, for $b = 2100, 800,$ and 400 km s^{-1} with $EW = 2.8 \text{ eV}$. $N_{\text{O VIII}} \sim 1 \times 10^{17} \text{ cm}^{-2}$ is close to the maximum column density predicted by Fang and Canizares (2000), who in-

vestigated the column density of the WHIM gas by Monte-Carlo simulations.

On the other hand, no O VII absorption line was detected. From the upper limit, the ionization fraction ratio of O VIII to O VII is constrained to be > 1.7 , assuming that both of the O VIII $K\alpha$ and O VII $K\alpha$ lines are not saturated. If we further assume collisional ionization equilibrium, this implies $kT > 0.20 \text{ keV}$ (Mazzotta et al. 1998). However, photoionization by the cosmic X-ray and UV background radiation would increase the ionization fraction of O VIII if the density is as low as 10^{-5} cm^{-3} (Chen et al. 2003). Since we can constrain only the upper limit of the density (see next paragraph), this could be the case for the WHIM around the Virgo cluster, and its temperature could be lower.

Excess emission was found in the EPIC spectra over the multi-component model representing the emission from the Virgo ICM, CXB, LHB, and MWH. The intensity of the multi-component model is consistent with the RASS diffuse soft X-ray background map in the north and the west regions just outside of the Virgo cluster. This strongly suggests that the excess emission is associated with the Virgo cluster. However, a possible contribution by emission from the North Polar Spur cannot be excluded completely. We thus take the emission intensity as the upper limit for the emission from the WHIM around the Virgo cluster. The O VIII column density is related to the average electron density, n_e , and the line-of-sight length, L , of the WHIM as $N_{\text{O VIII}} = fAZ_{\odot}n_eL$, where f is the ionization fraction, A is the oxygen abundance relative to the solar value, and Z_{\odot} is the solar abundance of the oxygen. On the other hand, if we assume a uniform distribution of the WHIM, the emission measure, EM, of the plasma is $EM \sim n_e^2LS$, where S is the geometrical area that we observed, and is $7.3 \times 10^3 \text{ kpc}^2$ for the present data. Then, the electron density and the line-of-sight distance are constrained to

$$n_e \lesssim 6 \times 10^{-5} \text{ cm}^{-3} \left(\frac{N}{1.5 \times 10^{-3}} \right) \left(\frac{A}{0.1} \right) \left(\frac{f}{0.4} \right) \quad (2)$$

$$\left(\frac{N_{\text{O VIII}}}{6.2 \times 10^{16} \text{ cm}^{-2}} \right)^{-1},$$

$$L \gtrsim 9 \text{ Mpc} \left(\frac{N}{1.5 \times 10^{-3}} \right)^{-1} \left(\frac{A}{0.1} \right)^{-2} \left(\frac{f}{0.4} \right)^{-2} \quad (3)$$

$$\left(\frac{N_{\text{O VIII}}}{6.2 \times 10^{16} \text{ cm}^{-2}} \right)^2,$$

where N is the normalization of the excess emission (see table 3), and 0.4 is the ionization fraction for $kT = 0.21 \text{ keV}$. The derived density corresponds to a baryon overdensity of $\delta \lesssim 250$. The depth of $\gtrsim 9 \text{ Mpc}$ is much larger than the linear dimensions of the Virgo cluster in the sky, but is consistent with the elongation of 12–30 Mpc suggested by Yasuda, Fukugita, and Okamura (1997), which is understood as being a filament of the large-scale hierarchical structure along the line of sight. Note that the line broadening due to the Hubble flow of the 9 Mpc line-of-sight distance corresponds to about

1.4 eV. This is much smaller than the 90% upper limit of the line width obtained from the present data. However, it could be resolved if the statistics were good enough, since it is comparable to the energy resolution of the RGS (~ 2 eV FWHM).

In summary, the present results strongly suggest the presence of the WHIM in a filament associated with the Virgo cluster at the 96.4% confidence level. To further constrain the physical parameters of the WHIM, a precise determination of the absorption line profile is an important next step. Future high-resolution spectroscopic observations of the emission are also strongly desirable for resolving the Galactic and extragalactic components.

We acknowledge Dr. Yuichirou Ezoe, who helped in the analysis of the RASS data. This work was supported in part by Grants-in-Aid for Scientific Research by MEXT/JSPS (14204017, 12440067, and 15340088).

References

- Bristow, P.D., & Philipps, S. 1994, *MNRAS*, 267, 13
 Burles, S., Nollett, K.M., & Turner, M.S. 2001, *ApJ*, 552, L1
 Cash, W. 1979, *ApJ*, 228, 939
 Cen, R., & Ostriker, J.P. 1999, *ApJ*, 514, 1
 Chen, X., Weinberg, D.H., Katz, N., & Davé, R. 2003, *ApJ*, 594, 42
 Davé, et al. 2001, *ApJ*, 552, 473
 Fang, T., & Canizares, C.R. 2000, *ApJ*, 539, 532
 Fang, T., Marshall, H.L., Lee, J.C., Davis, D.S., & Canizares, C.R. 2002, *ApJ*, 572, L127
 Fang, T., Sembach, K.R., & Canizares, C.R. 2003, *ApJ*, 586, L49
 Finoguenov, A., Briel, U.G., & Henry, J.P. 2003, *A&A*, 410, 777
 Fukugita, M., Hogan, C.J., & Peebles, P.J.E. 1998, *ApJ*, 503, 518
 Futamoto, K., Mitsuda, K., Takei, Y., Fujimoto, R., & Yamasaki, N.Y. 2004, *ApJ*, 605, 793
 den Herder, J.W., et al. 2001, *A&A*, 365, L7
 Hewett, P.C., Foltz, C.B., & Chaffee, F.H. 1995, *AJ*, 109, 1498
 Irwin, J.A., & Sarazin, C.L. 1996, *ApJ*, 471, 683
 Jansen, F., et al. 2001, *A&A*, 365, L1
 Kaastra, J.S., Lieu, R., Tamura, T., Paerels, F.B.S., & den Herder, J.W. 2003, *A&A*, 397, 445
 Lumb, D.H., Warwick, R.S., Page, M., & De Luca, A. 2002, *A&A*, 389, 93
 Mazzotta, P., Mazzitelli, G., Colafrancesco, S., & Vittorio, N. 1998, *A&AS*, 133, 403
 McKernan, B., Yaqoob, T., Mushotzky, R., George, I.M., & Turner, T.J. 2003, *ApJ*, 598, L83
 Nicastro, F., et al. 2002, *ApJ*, 573, 157
 Perna, R., & Loeb, A. 1998, *ApJ*, 503, L135
 Persic, M., & Salucci, P. 1992, *MNRAS*, 258, 14
 Rasmussen, A., Kahn, S.M., & Paerels, F. 2003, in *The IGM/Galaxy Connection: The Distribution of Baryons at z=0*, ed. J.L. Rosenberg & M.E. Putnam (Dordrecht: Kluwer Academic Publishers), 109
 Rauch, M., et al. 1997, *ApJ*, 489, 7
 Sarazin, C.L. 1989, *ApJ*, 345, 12
 Shibata, R., Matsushita, K., Yamasaki, N.Y., Ohashi, T., Ishida, M., Kikuchi, K., Röhringer, H., & Matsumoto, H. 2001, *ApJ*, 549, 228
 Snowden, S.L., et al. 1997, *ApJ*, 485, 125
 Spergel, D.N., et al. 2003, *ApJS*, 148, 175
 Verner, D.A., Verner, E.M., & Ferland, G.J. 1996, *Atomic Data Nucl. Data Tables*, 64, 1
 Voges, W., et al. 1999, *A&A*, 349, 389
 Yasuda, N., Fukugita, M., & Okamura, S. 1997, *ApJS*, 108, 417